

Temperature determination using $K\alpha$ spectra from M -shell Ti ions

S. B. Hansen,¹ A. Ya. Faenov,² T. A. Pikuz,² K. B. Fournier,¹ R. Shepherd,¹ H. Chen,¹ K. Widmann,¹ S. C. Wilks,¹ Y. Ping,¹ H. K. Chung,¹ A. Niles,¹ J. R. Hunter,¹ G. Dyer,³ and T. Ditmire³

¹Lawrence Livermore National Laboratory, P.O. Box 808, L-473, Livermore, California 94550, USA

²Multicharged Ions Spectra Data Center of VNIIFTRI, Mendeleev, Moscow region 141570, Russia

³Physics Department, University of Texas at Austin, Austin, Texas 78712, USA

(Received 25 March 2005; published 15 September 2005)

The compact multipulse terawatt (COMET) laser facility at LLNL was used to irradiate Al-coated 2–50 μm Ti foils with $\approx 10^{19}$ W cm^{-2} , 500 fs, 3–6 J laser pulses. Laser-plasma interactions on the front side of the target generate hot electrons with sufficient energy to excite inner-shell electrons in Ti, creating $K\alpha$ emission which has been measured using a focusing spectrometer with spatial resolution aimed at the back surface of the targets. The spatial extent of the emission varies with target thickness. The high spectral resolution ($\lambda/\Delta\lambda \approx 3800$) is sufficient to measure broadening of the $K\alpha$ emission feature due to the emergence of blueshifted satellites from ionized Ti in a heated region of the target. A self-consistent-field model is used to spectroscopically diagnose thermal electron temperatures up to 40 eV in the strongly coupled Ti plasmas.

DOI: [10.1103/PhysRevE.72.036408](https://doi.org/10.1103/PhysRevE.72.036408)

PACS number(s): 52.50.Jm, 32.70.-n, 52.70.La, 52.25.Jm

K -shell emission measurements are among the most widely used and reliable spectroscopic plasma diagnostics. The resonance $1s$ - $2p$ transitions in H- and He-like ions and their Li-like satellites have long been used as diagnostics of electron temperatures and densities in hot plasmas [1,2], and K -shell emission from L -shell ions has also proven useful in determining plasma properties [3–6]. At the other extreme of ionization, measurements of characteristic (or “cold”) $K\alpha$ yields from near-neutral ions have been powerful diagnostics for laser plasmas [7–9], where their high transition energies help to isolate the effects of hot electrons formed by laser-plasma interactions from the effects of thermal processes. Diagnostics based on spectroscopically resolved $K\alpha$ emission from M -shell ions [10] are not yet well developed but are of particular interest in the study of warm, dense matter.

The highly coupled plasmas in the warm, dense matter regime pose fundamental challenges to spectroscopic modeling in the form of density effects such as continuum lowering and quasibound states. For studies of mid- and high- Z materials, this regime also poses a practical challenge due to the complexity of many-electron ions that dominate in few-times ionized plasmas. Since shifts in the $K\alpha$ lines to higher energies are relatively small under the ionization of M -shell electrons, measurements with high spectral resolution are required in order to extract information about the ionization stages (and thence temperatures) present in an emitting plasma. In this paper, we present $K\alpha$ emission measurements with spatial and high spectral resolution from M -shell Ti ions and introduce a self-consistent-field model for ions in dense plasmas that can extract thermal temperatures from the measured spectra.

The experiments were conducted on the compact multipulse terawatt (COMET) laser facility at the Lawrence Livermore National Laboratory [11], a hybrid chirped pulse amplification (CPA) system consisting of a Ti:sapphire oscillator and regenerative amplifier tuned to 1054 nm wavelength with a four-stage Nd:phosphate glass amplifier. To obtain the present data, 3–6 J of laser energy were delivered to the target in a 500 fs pulse, which was focused by an

off-axis parabola to a spot size of ≈ 10 μm full width at half maximum (FWHM) at an incident angle of 45° . The nominal laser intensity reached 10^{19} W cm^{-2} , and the contrast of the laser pulse (the ratio between the peak intensity and the intensity 5 ps before the peak) was about 10^6 . The targets were Ti foils between 2 and 50 μm thick and were coated on the front (laser-irradiated) surface with 1000 \AA of Al. The Al coating absorbs the small amount of energy in the laser prepulse, prevents direct laser heating of the Ti target, and acts as a tamper to the Ti foil over the short duration of the main laser pulse. The tamping ensures that the back surface of the targets remains near solid density over the few-ps time scale of $K\alpha$ emission (as measured by a time-resolved Von Hamos spectrometer aimed at the front of the targets).

Spatially resolved x-ray spectra were measured using a focusing spectrometer with spatial resolution (FSSR-1D) [12,13] equipped with a spherically bent quartz crystal ($R = 150$ mm, $2d_{21\bar{3}0} \approx 3.082$ \AA) and a vacuum-compatible, back-illuminated charge-coupled-device (CCD) camera. The spectrometer viewed the back surface of the target at an angle of $\approx 30^\circ$ to the horizontal and $\approx 20^\circ$ to the vertical relative to the laser axis (see Fig. 1). For observation of the $K\alpha$ spectral lines of Ti, the spherically bent crystal was placed 225 mm from the plasma source and centered at $\lambda = 2.73$ \AA (Bragg angle $\theta = 63.3^\circ$). To record the emission, the CCD camera was placed on the Rowland circle 135.8 mm from the crystal. The spatial resolution of the spectrometer in this configuration was 48 μm in the horizontal plane of the target, and the spectral resolution on the CCD was $\lambda/\Delta\lambda \approx 3800$. It should be emphasized that because the crystal had a spherical shape and the detector was placed on the Rowland circle, the spectral resolution was not sensitive to the source size of the plasma.

Figure 1 shows the experimental setup along with FSSR-1D images from four Al-coated Ti foils of various thicknesses. Table I summarizes the characteristics of the target, laser, and measured $K\alpha$ emission from the four shots shown in Fig. 1. The transmission of characteristic (4510 eV) $K\alpha$ radiation through a cold Ti foil is also given.

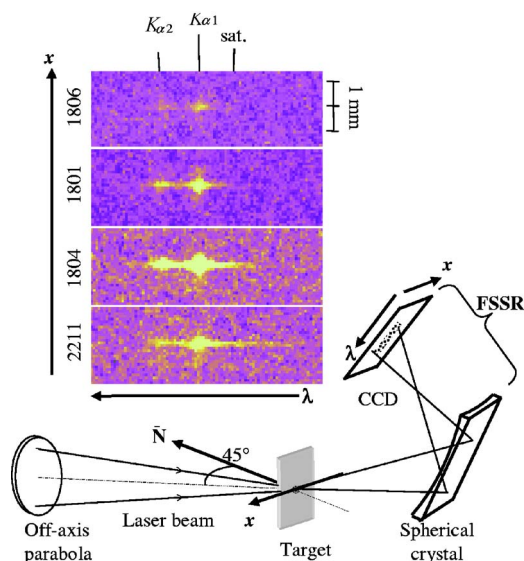


FIG. 1. (Color online) Scheme of experimental setup and images from four shots obtained by the FSSR spectrometer from the back surface of Al-coated Ti targets.

The $K\alpha_2$ emission film counts and the size of the $K\alpha_2$ emission region are correlated in Table I: both increase from the 2 μm target to the 12.5 μm target and then decrease with increasing target thickness. This implies that there is an optimal target thickness for maximum $K\alpha$ intensity. The measured emission extents are consistent with recent measurements of Ti $K\alpha$ yield with high spatial resolution from buried-layer targets, [10] with rear-side reflectivity measurements of fast-electron-heated targets,[14] and also with the $\approx 100 \mu\text{m}$ mean free path through solid Ti of few-hundred-keV electrons (a 100–200 keV hot electron distribution was measured with an electron spectrometer aimed at the back surface of the target).

Satellites on the high-energy side of the $K\alpha_1$ line, which come from ionized Ti in a heated region of the target, are clearly evident in the images in Fig. 1 for all but the 50 μm foils. The $\approx 100 \mu\text{m}$ spatial extent of the blue shifted satellites is smaller than the $\approx 200 \mu\text{m}$ extent of the unshifted characteristic $K\alpha$ emission and is consistent with collisional heating by lower-energy (50–100 keV) components of the measured hot-electron distribution.

Hydrodynamic simulations [15] without hot electrons were carried out to assess the importance of radiative heating and thermal conduction. The simulations of 2–25 μm Ti foil targets coated with 0.1 μm of Al irradiated by a 500 fs, 4 J laser pulse (with no prepulse) show a shock front moving at $\approx 0.3 \mu\text{m}/\text{ps}$ into the target, heating the material behind it to 100–200 eV. The fourfold compression of Ti in the simulated shock front is insufficient to pressure-ionize the 3*p* subshell and cannot account for the observed $K\alpha$ shifts. Radiation temperatures of 20–50 eV driven by emission from hot Al blowoff plasma run ahead of the shock front by several μm , consistent with the fast radiative heating of laser-irradiated foils described in [16]. However, since the spread of both the radiative and shock heating fronts along the target surface is less than 20 μm over 10 ps, these processes alone cannot account for the observed extent of the heated material.

To analyze the measured $K\alpha$ spectra, a self-consistent-field model [17–21] of ions in dense plasmas (MUZE) has been developed. The model describes the distribution of electrons in an average atom within a Wigner-Seitz cell whose radius R_0 is determined by the solid-Ti ion density ($n_i = 5.7 \times 10^{22} \text{ cm}^{-3}$). Neighboring ions restrict the size of the ion sphere and provide a uniform background charge density. Nonrelativistic bound and free wave functions for the average atom are calculated in an initial potential and are populated according to Fermi statistics, with cell neutrality ensured by variation of the chemical potential μ . The electron density so calculated is used to generate a new potential through Poisson’s equation with local density exchange and correlation effects following Rozsnyai [17]. The procedure is repeated until self-consistent solutions for the wave functions and potential are obtained.

Ion-in-cell models of this type give two choices for the average ion charge $\langle Z \rangle$: the number of electrons on the surface of the ion sphere Z_{free} and the number of continuum electrons Z_{cntm} , which includes both free electrons and quasibound electrons in continuum resonances and which can be discontinuous under pressure ionization of valence orbitals. In transition metals, Z_{free} and Z_{cntm} can differ by several electrons. To ensure a smooth variation of the average ion charge and to account for the effect of quasibound states, we use $\langle Z \rangle = Z_{\text{free}}$.

Next, the average atom is split into individual ions, with wave functions calculated within the Wigner-Seitz cell using

TABLE I. Characteristics of four shots including the thickness d of the target Ti foil, the incident laser intensity, the relative $K\alpha_2$ emission intensity, the emission extent Δx of the $K\alpha_2$ line and high-energy satellites, and the transmission of 4510 eV $K\alpha$ radiation through a cold Ti foil of thickness d . (Because the $K\alpha_1$ line was saturated on the film in shots 1804 and 2211, emission extents and relative counts on film are given only for $K\alpha_2$.)

Shot	Ti foil d (μm)	Laser int. ($\times 10^{19}$ W/cm ²)	$K\alpha_2$ counts on film	$K\alpha_2$ Δx (μm)	Sat. Δx (μm)	Cold Ti transm.
2211	2.0	0.87	0.61	150	100	0.91
1804	12.5	1.22	1.00	250	150	0.54
1801	25	0.61	0.77	200	100	0.29
1806	50	1.25	0.51	100	-	0.09

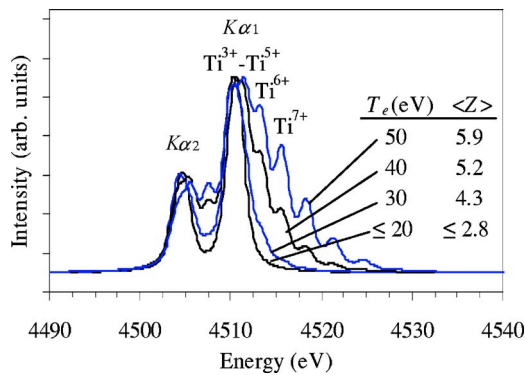


FIG. 2. (Color online) Modeled $K\alpha$ spectra and self-consistent $\langle Z \rangle$ at various electron temperatures. Increasing ionization gives rise to a blue wing on the characteristic $K\alpha_1$ line and fills in the gap between the cold $K\alpha_1$ and $K\alpha_2$ lines.

potentials optimized to the ground-state configuration of each ion. The continuum charge density is not included in the calculation of individual ion potentials since the effects of quasibound states are included in the definition of the average ion charge. Approximate relativistic corrections are added to the bound-state energies to account for the splitting between $K\alpha_1$ and $K\alpha_2$ and a single global correction is added to the calculated transition energies [22] so that the cold $K\alpha$ line matches tabulated values [23]. Electric-dipole oscillator strengths are computed using the average atom wave functions and scaled to the transition energies of individual ions, and the charge-state distribution is determined by enforcing Saha-Boltzmann equilibrium. Synthetic spectra are constructed using Voigt line shapes which convolve the nominal instrumental resolution with a Voigt parameter of unity. Line intensities are taken to be proportional to the parent ion population, the radiative decay rate, and the statistical weight of the upper level.

Results of the MUZE model for temperatures from 20 to 50 eV are given in Fig. 2. As T_e increases and the Ti atoms ionize, satellite lines emerge on the high-energy side of the $K\alpha_1$ line, giving the appearance of a blue wing, and satellites to the $K\alpha_2$ transition fill in the gap between the cold characteristic lines. The charge states of selected $K\alpha_1$ satellites are indicated on the figure: lines from Ti^{3+} to Ti^{5+} all lie between 4510 and 4512 eV, while lines from Ti^{6+} and higher charge states each exhibit a 2-3 eV blueshift with each ionized $3p$ electron. Transitions with excited spectator electrons are not explicitly included in the MUZE model, even though they can broaden and shift the emission feature from a single ion [24]. Instead, since the majority of excited states with spectator holes lie above the continuum limit, satellites of the kind described in Ref. [25] are simply taken to belong to a more highly charged ion.

To test the accuracy of the wavelengths in the MUZE model and to verify the assumption of local thermodynamic equilibrium (LTE), we have compared our results to those of a collisional-radiative model [26] for Ti^{3+} to Ti^{7+} based on data from the relativistic multiconfiguration atomic structure code FAC [27]. (Neutral Ti to Ti^{2+} are pressure ionized in MUZE at solid density, so no comparison could be made with the isolated-ion calculations of FAC.) FAC predicts many hun-

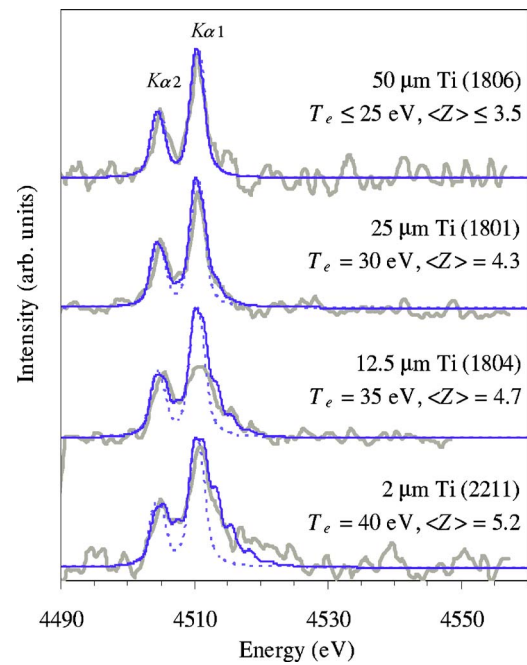


FIG. 3. (Color online) Experimental spectra (gray lines) exhibit increasing departures from the characteristic “cold” $K\alpha$ emission feature (dashed lines) as the target thickness decreases from 50 μm to 2 μm . The best-fit modeled spectra (solid lines) imply increasing temperatures with decreasing target thickness.

dreds of lines from each ion even in the density-restricted configuration space, but the dominant emission features generally retain the dual-peak shape of the characteristic $K\alpha$ lines and agree to within 1–2 eV with the MUZE calculations. We note that both FAC and MUZE calculate redshifts in moving from Ti^{3+} to Ti^{4+} , which were first predicted by House [22] and later observed in high-resolution measurements from vacuum spark plasmas [28,29]. The collisional-radiative model calculations confirm that solid density conditions are sufficient to enforce LTE and that the ionization balance determined by the thermal electron temperature is practically unaffected by hot-electron fractions less than a few percent [6].

We emphasize that the MUZE model has two important advantages over highly detailed isolated-ion structure codes. On a fundamental level, density effects such as continuum lowering and the exclusion of quasibound states from the average ion charge are intrinsically included in the MUZE model, so there is need to impose external corrections. A more practical advantage is the simplified atomic structure of the MUZE model, which translates to an orders-of-magnitude reduction in computational complexity for the M -shell ions considered here.

Figure 3 shows experimental lineouts of the central 200 μm portion of the images shown in Fig. 1. The lineouts have been smoothed to the nominal spectral resolution to minimize instrumental noise. As the target thickness decreases, the experimental spectra exhibit clear departures from the cold $K\alpha$ emission feature characterized by a broadening of both the $K\alpha_1$ and $K\alpha_2$ lines to the blue, which results in the emergence of a high-energy wing on $K\alpha_1$ and

a filling in of the gap between $K\alpha_1$ and $K\alpha_2$. To quantitatively diagnose temperatures corresponding to the observed broadening, we normalized modeled spectra to the unsaturated $K\alpha_2$ line and varied the temperature to obtain the best fit to the shape of the experimental spectra. For the present data, this diagnostic has a precision of ± 5 eV for $T_e > 25$ eV. The diagnosed thermal temperatures increase from less than 25 eV for the thickest foil to 40 eV for the thinnest. At these conditions, the plasma is strongly coupled, with an ion-ion coupling parameter $\Gamma_{ii} = \langle Z \rangle^2 / R_0 k_B T_e$ between 4 and 6.

As noted above, the difference in the spatial extent of the warm-Ti satellites and the characteristic (cold) $K\alpha$ emission indicates that the temperature decreases in the radial direction along the surface. Since the lineouts given in Fig. 3 average over that temperature gradient, temperatures higher than the diagnosed T_e may exist. The present measurements also represent a transmission-modulated average in the direction perpendicular to the surface of the target, along which temperature gradients have been observed in similar experiments [4]. If one sets the temperature to be 40 eV in the first $\approx 10 \mu\text{m}$ of the $> 2 \mu\text{m}$ foils and zero in the remainder, the total emission (including absorption) closely resembles the best-fit optically thin spectra given in Fig. 3. Thus the present diagnostics can be taken either to represent an average tem-

perature over the foil thickness or as estimates of the temperature gradient scale length. Buried-layer targets could eliminate the ambiguity.

In summary, we have presented $K\alpha$ emission measurements taken from the back surface of Al-coated Ti foils of varying thickness irradiated by a high-intensity laser and have introduced a self-consistent-field model for use as a temperature diagnostic of warm, dense matter. Spatial variations in the $K\alpha$ spectra indicate temperature gradients parallel to the surface of the target material over $\approx 100 \mu\text{m}$ length scales. The high spectral resolution of the measurements has enabled the identification of $K\alpha$ emission from 6–8-times-ionized Ti, indicating temperatures of at least 40 eV in the first few μm of the tamped Ti target and decreasing average T_e with increasing target thickness.

We thank Brian Wilson, Jim Albritton, and Vijay Sonnad for helpful discussions about the modeling approach. This work was performed under the auspices of the U.S. Department of Energy by University of California Lawrence Livermore National Laboratory under Contract No. W-7405-Eng-48 (LDRD 04-ERD-023). The work of A.F. and T.P. was supported by INTAS (Grant No. 01-0233).

-
- [1] A. H. Gabriel, *Mon. Not. R. Astron. Soc.* **160**, 99 (1972).
 [2] D. Duston and J. Davis, *Phys. Rev. A* **21**, 1664 (1980).
 [3] S. Morita and J. Fujita, *Appl. Phys. Lett.* **43**, 443 (1983).
 [4] H. Chen, B. Soom, B. Yaakobi, S. Uchida, and D. D. Meyerhofer, *Phys. Rev. Lett.* **70**, 3431 (1993).
 [5] J. Abdallah, Jr. *et al.*, *J. Quant. Spectrosc. Radiat. Transf.* **62**, 85 (1999).
 [6] T. Kawamura *et al.*, *Phys. Rev. E* **66**, 016402 (2002); H. Nishimura *et al.*, *J. Quant. Spectrosc. Radiat. Transf.* **81**, 327 (2003). H. Nishimura *et al.*, *ibid.* **87**, 211 (2004).
 [7] J. D. Hares, J. D. Kilkenny, M. H. Key, and J. G. Lunney, *Phys. Rev. Lett.* **42**, 1216 (1979).
 [8] U. Tuebner *et al.*, *Phys. Rev. E* **54**, 4167 (1996).
 [9] R. B. Stephens *et al.*, *Phys. Rev. E* **69**, 066414 (2004).
 [10] V. Decaux, P. Beiersdorfer, A. Osterheld, M. Chen, and S. M. Kahn, *Astrophys. J.* **443**, 464 (1995).
 [11] J. Dunn, Y. Li, A. L. Osterheld, J. Nilsen, J. R. Hunter, and V. N. Shlyaptsev, *Phys. Rev. Lett.* **84**, 4834 (2000).
 [12] A. Ya. Faenov *et al.*, *Phys. Scr.* **50**, 333 (1994).
 [13] I. Yu. Skobelev *et al.*, *Zh. Eksp. Teor. Fiz.* **108**, 1263 (1995) [*JETP* **81**, 692 (1995)].
 [14] E. Martinolli *et al.*, *Phys. Rev. E* **70**, 055402(R) (2004).
 [15] G. Zimmerman and W. Kruer, *Comments Plasma Phys. Controlled Fusion* **2**, 85 (1975).
 [16] D. Duston, R. W. Clark, J. Davis, and J. P. Apruzese, *Phys. Rev. A* **27**, 1441 (1983).
 [17] B. Rozsnyai, *Phys. Rev. A* **5**, 1137 (1972).
 [18] W. R. Johnson, C. Guet, and G. F. Bertsch (unpublished).
 [19] D. A. Liberman, *Phys. Rev. B* **20**, 4981 (1979).
 [20] R. Cauble, M. Blaha, and J. Davis, *Phys. Rev. A* **29**, 3280 (1984).
 [21] J.-C. Pain and T. Blenski, *J. Quant. Spectrosc. Radiat. Transf.* **81**, 355 (2003).
 [22] L. L. House, *Astrophys. J., Suppl.* **18**, 21 (1969).
 [23] J. A. Bearden, *Rev. Mod. Phys.* **39**, 78 (1967).
 [24] J. J. MacFarlane, P. Wang, J. Bailey, T. A. Mehlhorn, R. J. Dukart, and R. C. Mancini, *Phys. Rev. E* **47**, 2748 (1993).
 [25] N. Shigeoka, H. Oohashi, T. Tochio, Y. Ito, T. Mukoyama, A. M. Vlaicu, and S. Fukushima, *Phys. Rev. A* **69**, 052505 (2004).
 [26] S. B. Hansen, Ph.D dissertation, University of Nevada, Reno, 2003.
 [27] M. F. Gu, *Astrophys. J.* **590**, 1131 (2003); **582**, 1241 (2003).
 [28] E. V. Aglitskii, E. Ya. Gol'ts, M. N. Driker, L. N. Ivanov, Yu. A. Levykin, and A. M. Livshits, *J. Phys. B*, **15**, 2001 (1982).
 [29] S. Morita, K. Kadota, T. Kagawa, and J. Fujita, *Phys. Lett.* **94A**, 147 (1983).